Wrench Capability Analysis of a Planar Dual-Platform Cable-Driven Parallel Robot

Tahir Rasheed, Philip Long, Taşkin Padir, Stéphane Caro

Proceedings of the ASME 2023 International Design Engineering Technical Conferences & Computers and Information in Engineering Conference
IDETC/CIE 2023
August 20-23, 2023, Boston, Massachusetts, USA

IDETC2023-116412

WRENCH CAPABILITY ANALYSIS OF A PLANAR DUAL-PLATFORM CABLE-DRIVEN PARALLEL ROBOT

Tahir Rasheed[1], Philip Long[2], Taskin Padir[3], Stephane Caro[1]
[1] Nantes Universite, Ecole Centrale Nantes, CNRS, LS2N, UMR 6004, F-44000 Nantes, France
[2] Atlantic Technological University, Galway, Ireland
[3] Northeastern University College of Engineering, Boston, United States
Emails: Tahir.Rasheed@univ-nantes.fr, philip.long@atu.ie,
t.padir@northeastern.edu, Stephane.Caro@ls2n.fr

ABSTRACT

Cable-Driven Parallel Robots have several advantages over both conventional serial and parallel robots, notably in terms of scalable workspace. These robots could provide an alternative to mobile and gantry crane systems, increasing payload stability, allowing higher accelerations and reducing cost. However, in order to provide such capabilities, the base attachment points must be located outside the workspace boundaries, meaning that the cables form straight lines running through the workspace to the mobile platform. Consequently, such systems can only feasibly operate in unencumbered locations, or alternatively, be configured with a specific task in mind thus severely limiting their functionality. One potential solution to this problem is a composite mechanism that docks then deploy a sub-mechanism. In this paper, a methodology is proposed to obtain the Wrench-Feasible-Workspace of a composite Cable-Driven Parallel Robot by determining its Available Wrench Set. We define three operation modes of such system and show that the Available Wrench Set in each operation mode depends on the static equilibrium of the dual-platform and contact conditions. The Available Wrench Set is constructed by the Hyperplane Shifting Method and is validated in simulation.

1 Introduction

Cable-Driven Parallel Robots (CDPRs) are a type of parallel robot in which a set of cables connect a mobile platform equipped with an end-effector to fixed attachment points on the boundary of the workspace. Each cable is taut and allows forces to be transmitted from fixed motorized winches to the moving-platform. The absence of rigid links means the system must be redundantly actuated to ensure the platform to be fully controllable. However, this in turn means the system is much lighter and easily reconfigurable enabling potential applications in high acceleration tasks [1], large outdoor applications [2], logistics [3] and physiotherapy [4].

In spite of the evident advantages of cable actuated systems, several challenges have limited their deployment in the real-world applications. Foremost amongst these challenges, is the issue of collision avoidance between the cables and the environment and as a consequence limiting the robot's feasible workspace [5]. While permitting cable collisions can lead to a larger workspace, such incidents require on-line adjustment of the robot model [6] and could lead to costly failures. Therefore, much work has focused on detecting potential collisions [7] requiring significant computational effort [8]. The collision detection algorithms can then be used in classical path planning methods, for example, discrete methods [9] or sampling based algorithms e.g, *RRT* [10,11]. These approaches are computationally intensive, thus alternative methods have been sought. For instance, if the desired task is known, a collision free workspace can be directly used as a design parameter for the robot's structure [12], an efficient yet specific method.

To overcome this limitations, Reconfigurable Cable-

Driven Parallel Robots (RCDPRs), have been proposed [13]. RCDPRs allow reconfiguration of the base attachment points to alter the characteristics of the robot. Planning algorithms can then be used to select the optimum configuration [14] for a particular task. Yet, these systems require discrete manual reconfiguration and thereby limiting the system to known static environments. Alternatively the attachment points can be attached to mobile devices [3, 15] creating systems which can be deployed or reconfigured easily and in an automatic fashion. The addition of mobile bases introduces supplementary constraints that must be considered in the formulation of the robot's wrench set [16] and requires novel tension distribution algorithms [17]. Such RCDPRs would be capable of navigating to the desired location [18, 19] and deploying a suitable robot *on-demand* for a specific task.

While, adding a high level of flexibility, RCDPRs still struggle to perform in a cluttered workspace due to cable collisions, for instance loading and unloading containers. To address this issue, a novel robot is proposed in [20] composed of a suspended CDPR, a composite mobile platform and a docking mechanism. The proposed system is designed to move above a cluttered environment and when latched deploys a sub-mechanism, which can descend between the obstacles. Collisions are avoided as the cables are routed through the docked system. The docking mechanism consists of two parts a fixed beam at the top of the workspace and a latching mechanism. This mechanism, inspired by a retractable pen [21], converts a vertical translational into incremental rotations, enabling by a unidirectional force to dock and undock the robot. This system is complex and requires particular infrastructure in the workspace. Inspired by this work in this paper, we build on the idea of sub-mechanisms and present a new concept of multiple moving-platforms CDPR. Each platform is connected to its independent cables. Rather than a docking system, we propose a sub-mechanism that can be deployed by appropriate tension distribution and surface contact, thus eliminating the complex latching mechanism and broadening the applicability of the system. The proposed system combines the advatages of a CDPR with the flexibility of a standard crane system.

In this article, only two platforms are considered denoted as platform 1 ($\mathscr{P}_1$) and platform 2 ($\mathscr{P}_2$) as illustrated in Fig. 2. An ongoing development of a dual-platform CDPR using the CRAFT prototype is shown in Fig. 1. This paper deals with the determination of the Available Wrench Set (AWS) required to trace the workspace for planar CDPRs with dual point-mass end-effector. Figure 2 illustrates a Planar CDPR (PCDPR) with $q = 4$ cables and $n = 2$ DoF dual moving-platforms. This paper is organized as follows. Section 2 presents the parameterization of the robot. Section 3 deals with the Static Equilibrium (SE) conditions of the robot using Free Body Diagram (FBD). Section 4 discusses the nature of AWS by consid-

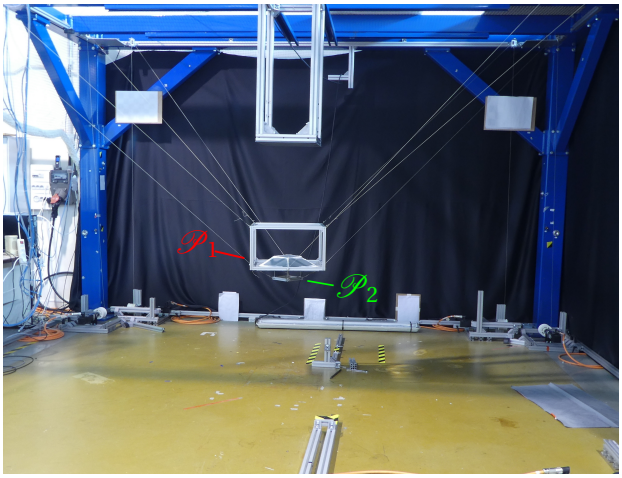

(a) first mode of operation

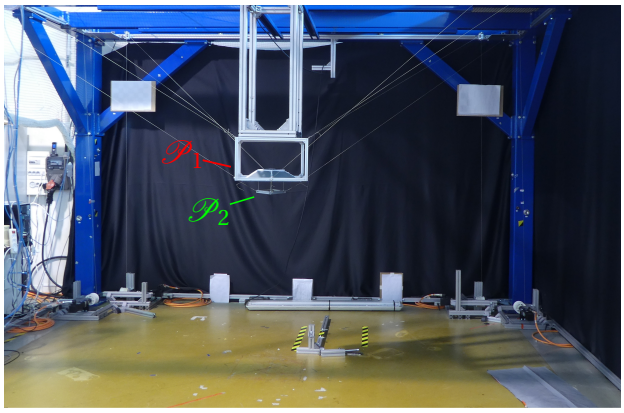

(b) second mode of operation

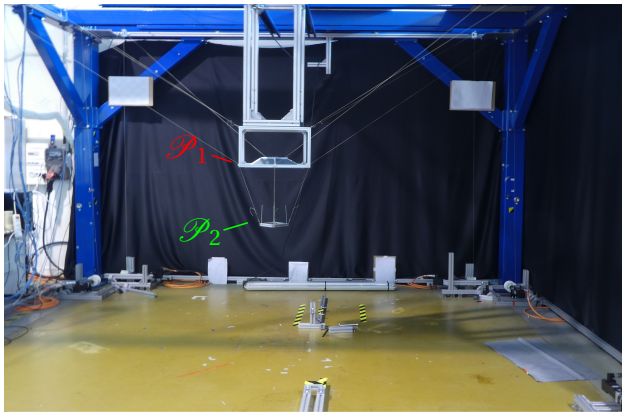

(c) third mode of operation

FIGURE 1: Ongoing developments of a dual-platform mechanism using the CRAFT prototype located at LS2N, Nantes, France.

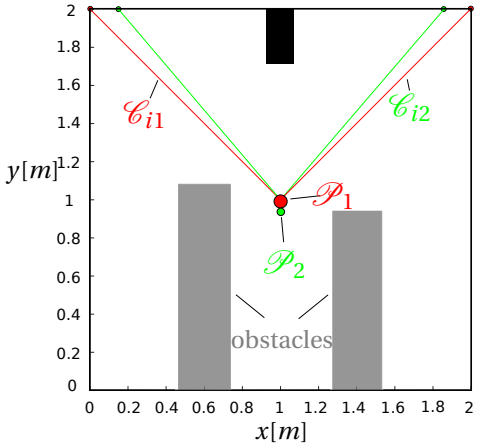

(a) first mode of operation

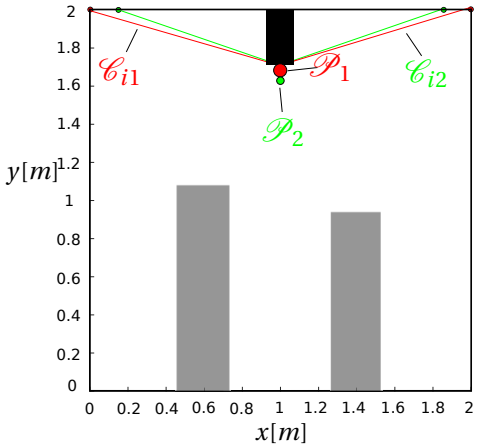

(b) second mode of operation

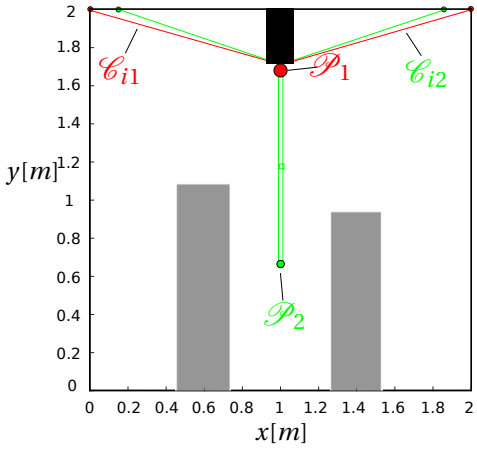

(c) third mode of operation

FIGURE 2: Dual-platform CDPR supported by $q_1 = 3$ and $q_2 = 3$ number of cables in three different operation modes (a) stowed (b) during docking (c) deployed

ering the SE of the platforms for each mode of operation. Section 5 discusses how to trace the workspace using the capacity margin index. Finally, conclusions are drawn and future work is presented in Section VI.

2 Robot Parameterization

The robot in Fig. 2a is named as dockbot. Dockbot is designed to have three modes of operation, two motion modes and one transitory static mode:

1. The first mode of operation occurs when both the platforms are in contact and are static relative to each other, yet free to move as one body within the workspace. The purpose of first mode of operation is to facilitate the maneuvering of the platforms in a cluttered environment and to precisely position them for attachment to the ceiling, as illustrated in the in Fig. 2a.
2. After the first mode of operation is completed, the second mode is initiated in which the platforms are static and in contact with each other, as well as docked against the ceiling. This mode, as depicted in Figure 2b, is specifically designed to maintain the docked position of the platforms and ensure they remain in place. It commences immediately after the first mode is finished.
3. The third mode of operation occurs when the platform $\mathscr{P}_1$ is docked against the ceiling while platform $\mathscr{P}_2$ is free to move in a sub-workspace, actuated by the cables *only* attached to platform $\mathscr{P}_2$. This mode, as illustrated in Figure 2c, is specifically designed to enable platform $\mathscr{P}_2$ to descend between obstacles and perform the desired task, *e.g.*, pick and place operation [20], while keeping platform $\mathscr{P}_1$ securely docked to the ceiling. This mode ensures that the desired configuration of $\mathscr{P}_1$ is maintained, while allowing for efficient descend of $\mathscr{P}_2$ for the desired application.

Let us denote the jth moving-platform as $\mathscr{P}_j, j = 1,2$. The ith cable supporting $\mathscr{P}_j$ is named as $\mathscr{C}_{ij}, i = 1,\ldots,q_j, j = 1,2$, where q_j denotes the number of cables connected by $\mathscr{P}_j$. The total number of cables, denoted by q, is equal to

$$q = \sum_{j=1}^{2} q_j. \tag{1}$$

Let $\mathbf{u}_{ij}$ be the unit vector of $\mathscr{C}_{ij}$ pointing from the moving-platform anchor point B_{ij} to the cable exit point A_{ij}. Let $\mathbf{t}_{ij}$ be the cable tension vector along $\mathbf{u}_{ij}$, expressed as

$$\mathbf{t}_{ij} = t_{ij}\mathbf{u}_{ij} \tag{2}$$

where t_{ij} is the tension in the ith cable attached to $\mathscr{P}_j$.

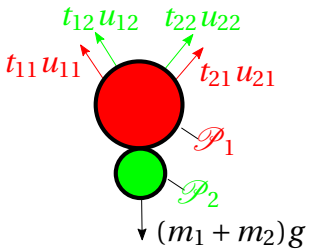

(a) FBD of the moving-platforms in the first mode

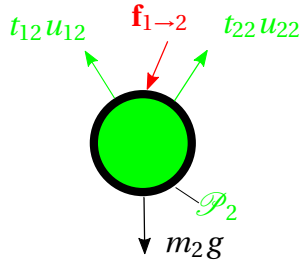

(b) FBD of $\mathscr{P}_2$ (for first mode)

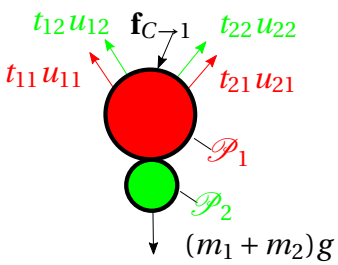

(c) FBD of the moving-platforms in the second mode

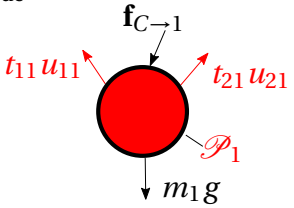

(d) FBD of $\mathscr{P}_1$ in the third mode

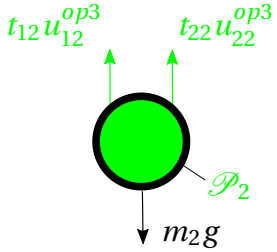

(e) FBD of $\mathscr{P}_2$ in the third mode

FIGURE 3: FBD of a dual moving-platform CDPR with $q_1 = 2$ and $q_2 = 2$ for the three operation modes.

3 Robot Modeling and Static Equilibrium

3.1 First Operation Mode

In the first operation mode, the two moving-platforms are in contact with no relative motion. From the FBD of both masses in Fig. 3a, the static equilibrium of the moving-platforms can be expressed as:

$$\mathbf{W}_1\mathbf{t}_1 + \mathbf{W}_2\mathbf{t}_2 + (m_1+m_2)\mathbf{g} = \mathbf{0}_2, \tag{3}$$

where,

$$\mathbf{W}_1 = \begin{bmatrix}\mathbf{u}_{11}\ \mathbf{u}_{21}\ \dots\ \mathbf{u}_{q_11}\end{bmatrix}, \quad \mathbf{W}_2 = \begin{bmatrix}\mathbf{u}_{12}\ \mathbf{u}_{22}\ \dots\ \mathbf{u}_{q_22}\end{bmatrix}, \tag{4}$$

$$\mathbf{t}_1 = \begin{bmatrix}\mathbf{t}_{11}\\ \mathbf{t}_{21}\\ \vdots\\ \mathbf{t}_{q_11}\end{bmatrix}, \ \mathbf{t}_2 = \begin{bmatrix}\mathbf{t}_{12}\\ \mathbf{t}_{22}\\ \vdots\\ \mathbf{t}_{q_22}\end{bmatrix} \tag{5}$$

$\mathbf{g} = [0,\ -g]^T$, where $g = 9.81\ m/s^2$. $\mathbf{u}_{ij}$ is the unit vector associated with $\mathscr{C}_{ij}$ pointing from the jth point mass moving-platform to the cable exit point. From the FBD of $\mathscr{P}_2$ in Fig. 3b, static equilibrium of $\mathscr{P}_2$ is expressed as:

$$\mathbf{W}_2\mathbf{t}_2 + m_2\mathbf{g} + \mathbf{f}_{1\to2} = \mathbf{0}_2. \tag{6}$$

where $\mathbf{f}_{1\to2}$ represents the reaction force applied by $\mathscr{P}_1$ on $\mathscr{P}_2$, can be expressed as:

$$\mathbf{f}_{1\to2} = -\mathbf{W}_2\mathbf{t}_2 - m_2\mathbf{g}. \tag{7}$$

Equation (3) shows the SE of a CDPR [1, 22] that only considers a single and point-mass moving-platform, *i.e.*, $\mathscr{P}_1$ and $\mathscr{P}_2$ joined together as a single body. It is the linear mapping from the q_1+q_2-dimensional cable tension space to a n-dimension wrench space. Equation (3) can also be expressed in the compact form as:

$$\mathbf{W}\mathbf{t} + \mathbf{w}_e = \mathbf{0}_2, \tag{8}$$

where $\mathbf{W}$ is a $n \times (q_1+q_2)$-dimensional matrix, $\mathbf{t}$ is (q_1+q_2)-dimensional column vector and $\mathbf{w}_e$ is a n-dimensional column vector denoting the external wrench applied to the end-effector, expressed as:

$$\mathbf{W} = \begin{bmatrix}\mathbf{W}_1\ \mathbf{W}_2\end{bmatrix}, \quad \mathbf{t} = \begin{bmatrix}\mathbf{t}_1\\ \mathbf{t}_2\end{bmatrix}, \quad \mathbf{w}_e = (m_1+m_2)\mathbf{g}. \tag{9}$$

The wrenches $\mathbf{f} = [f_x\ f_y]^T$ generated by the cables $\mathscr{C}_{ij}, i = 1,\ldots,q_j, j = 1,2$, onto the moving-platform is expressed as:

$$\mathbf{f} = \sum_{j=1}^{2}\sum_{i=1}^{q_j} t_{ij}\mathbf{u}_{ij} = \mathbf{W}_1\mathbf{t}_1 + \mathbf{W}_2\mathbf{t}_2. \tag{10}$$

$\mathbf{f}$ is the $n-$dimensional vector denoting the force generated by the cables on a dual-platform CDPR.

In the first operation mode, the two moving-platforms must remain in contact with no relative motion. The constrained can be modeled using the aforementioned reaction forces satisfying the non-sliding conditions defined by a friction cone [23, 24]. Thus, the non-sliding conditions expressed in the form of a friction cone are defined as:

$$|\mathbf{i}^T\mathbf{f}_{1\to2}| \leq -\mu\,\mathbf{j}^T\mathbf{f}_{1\to2}, \tag{11}$$

where μ denotes the friction coefficient between the two bodies. The negative sign in the above equation is due the fact that $\mathscr{P}_1$ must push $\mathscr{P}_2$ downward as shown in Fig. 3a in operation mode 1. Equation (11) expressed dual constraints that can be written as:

$$\mathbf{i}^T\mathbf{f}_{1\to2} \leq -\mu\,\mathbf{j}^T\mathbf{f}_{1\to2}, \tag{12a}$$

$$-\mathbf{i}^T\mathbf{f}_{1\to2} \leq -\mu\,\mathbf{j}^T\mathbf{f}_{1\to2}. \tag{12b}$$

where $\mathbf{i}$ and $\mathbf{j}$ denotes the unit vector along x and y axes, respectively.

3.2 Second Operation Mode

In the second operation mode depicted in Fig. 2b, both the moving-platforms must remain in contact and static relative to each other. In addition, the moving-platform $\mathscr{P}_1$ must also remain in contact with the ceiling. Thus in addition to the non-sliding conditions between the two moving-platforms expressed in Eq. (12), the non-sliding conditions between $\mathscr{P}_1$ and the ceiling needs to be respected as well.

From the FBD in Fig. 3c, the static equilibrium of $\mathscr{P}_2$ remains the same as expressed in Eq. (6) while the static equilibrium of $\mathscr{P}_1$ is expressed as,

$$\mathbf{W}_1\mathbf{t}_1 + \mathbf{W}_2\mathbf{t}_2 + (m_1+m_2)\mathbf{g} + \mathbf{f}^{o2}_{c\to1} = \mathbf{0}_2, \tag{13}$$

where $\mathbf{f}^{o2}_{c\to1}$ represents the reaction forces applied by the ceiling on $\mathscr{P}_1$ during the second mode of operation. Using Eq. (9), $\mathbf{f}^{o2}_{c\to1}$ can be expressed as:

$$\mathbf{f}^{o2}_{c\to1} = -\mathbf{W}\mathbf{t} - \mathbf{w}_e. \tag{14}$$

The non-sliding conditions between $\mathscr{P}_1$ and the ceiling introduces the limit on the reaction force $\mathbf{f}^{o2}_{c\to1}$, expressed as:

$$\mathbf{i}^T\mathbf{f}^{o2}_{c\to1} \leq -\mu\,\mathbf{j}^T\mathbf{f}^{o2}_{c\to1}. \tag{15a}$$

$$-\mathbf{i}^T\mathbf{f}^{o2}_{c\to1} \leq -\mu\,\mathbf{j}^T\mathbf{f}^{o2}_{c\to1}, \tag{15b}$$

3.3 Third Operation Mode

During the third mode of operation, the two platforms operate independently without any interaction between them, resulting in the generation of separate wrenches. Let $\mathbf{f}_j$ be the wrenches generated by the cables $\mathscr{C}_{ij}, i = 1,\ldots,q_j$ onto the jth moving-platform. In the third operation mode depicted in Fig. 2c, the moving-platform $\mathscr{P}_1$ must remain in contact only with the ceiling. From the FBDs in Figs. 3d and 3e, the static equilibrium of $\mathscr{P}_1$ and $\mathscr{P}_2$ can be expressed as:

$$\mathbf{W}_1\mathbf{t}_1 + m_1\mathbf{g} + \mathbf{f}^{o3}_{c\to1} = \mathbf{0}_2, \tag{16a}$$

$$\mathbf{W}_2\mathbf{t}_2 + m_2\mathbf{g} = \mathbf{0}_2. \tag{16b}$$

where,

$$\mathbf{W}_1\mathbf{t}_1 = \mathbf{f}_1, \qquad \mathbf{W}_2\mathbf{t}_2 = \mathbf{f}_2. \tag{17}$$

From Eq. (16a), the reaction force $\mathbf{f}^{o3}_{c\to1}$ between the ceiling and $\mathscr{P}_1$ is expressed as:

$$\mathbf{f}^{o3}_{c\to1} = -\mathbf{W}_1\mathbf{t}_1 - m_1\mathbf{g} \tag{18}$$

It can be observed that compared to $\mathbf{f}^{o2}_{c\to1}$, $\mathbf{f}^{o3}_{c\to1}$ only depends on the forces generated by the cables $\mathscr{C}_{i1}$ onto the platform $\mathscr{P}_1$. Similar to Eq. (15), the non-sliding conditions between $\mathscr{P}_1$ and the ceiling in the third mode of operation are expressed as:

$$\mathbf{i}^T\mathbf{f}^{o3}_{c\to1} \leq -\mu\,\mathbf{j}^T\mathbf{f}^{o3}_{c\to1}, \tag{19a}$$

$$-\mathbf{i}^T\mathbf{f}^{o3}_{c\to1} \leq -\mu\,\mathbf{j}^T\mathbf{f}^{o3}_{c\to1}. \tag{19b}$$

3.4 Cable tensions limits

Regardless of any operation mode of the CDPR, the constraints related to the lower and upper bounds on the cable tensions must be respected. The cable tension t_{ij} associated with the ith cable supporting the jth moving-platform is bounded between a minimum tension $\underline{t}_{ij}$ and a maximum tension $\overline{t}_{ij}$:

$$\underline{t}_{ij} \leq t_{ij} \leq \overline{t}_{ij}, \tag{20}$$

where t_{ij} is the ith cable tension connected to the jth body $\mathscr{P}_j$.

4 Available Wrench Set

In this section the nature of the AWS for a dual-platform CDPR is analyzed. It should be noted that the AWS of a classical CDPR depends uniquely on its platform pose and cable tension limits. In contrast, the additional conditions must be considered in the definition of the AWS for the dual-platform CDPR. Moreover, each mode of operation has different AWS depending on the additional constraints. Let $\mathscr{A}_1$ and $\mathscr{A}_2$ be the AWS associated with the first and second modes of operation, expressed as:

$$\mathscr{A}_1 = \left\{ \begin{array}{l} \mathbf{f} \in \mathbb{R}^2 \mid \mathbf{f} = \sum_{j=1}^{2} \sum_{i=1}^{q_j} t_{ij}\mathbf{u}_{ij},\ \ \underline{t}_{ij} \leq t_{ij} \leq \overline{t}_{ij}, \\ \mathbf{i}^T\mathbf{f}_{1\to 2} \ \leq\ -\mu\,\mathbf{j}^T\mathbf{f}_{1\to 2},\ \ -\mathbf{i}^T\mathbf{f}_{1\to 2} \ \leq\ -\mu\,\mathbf{j}^T\mathbf{f}_{1\to 2}, \\ \ \ i = 1,\ldots,q_j,\ \ j = 1,2. \end{array} \right. \tag{21}$$

$$\mathscr{A}_2 = \left\{ \begin{array}{l} \mathbf{f} \in \mathbb{R}^2 \mid \mathbf{f} = \sum_{j=1}^{2} \sum_{i=1}^{q_j} t_{ij}\mathbf{u}_{ij},\ \ \underline{t}_{ij} \leq t_{ij} \leq \overline{t}_{ij}, \\ \mathbf{i}^T\mathbf{f}_{1\to 2} \ \leq\ -\mu\,\mathbf{j}^T\mathbf{f}_{1\to 2},\ \ -\mathbf{i}^T\mathbf{f}_{1\to 2} \ \leq\ -\mu\,\mathbf{j}^T\mathbf{f}_{1\to 2}, \\ \mathbf{i}^T\mathbf{f}^{o2}_{c\to 1} \ \leq\ -\mu\,\mathbf{j}^T\mathbf{f}^{o2}_{c\to 1},\ \ -\mathbf{i}^T\mathbf{f}^{o2}_{c\to 1} \ \leq\ -\mu\,\mathbf{j}^T\mathbf{f}^{o2}_{c\to 1}, \\ \ \ i = 1,\ldots,q_j,\ \ j = 1,2. \end{array} \right. \tag{22}$$

In the third mode of operation, as the platforms operate independently, each platform has its own independent AWS. Let $\mathscr{A}_{3j}$ be the AWS associated with the jth platform in the third mode of operation, expressed as:

$$\mathscr{A}_{31} = \left\{ \begin{array}{l} \mathbf{f}_1 \in \mathbb{R}^2 \mid \mathbf{f}_1 = \sum_{i=1}^{q_1} t_{i1}\mathbf{u}_{i1},\ \ \underline{t}_{i1} \leq t_{i1} \leq \overline{t}_{i1}, \\ \mathbf{i}^T\mathbf{f}^{o3}_{c\to 1} \ \leq\ -\mu\,\mathbf{j}^T\mathbf{f}^{o3}_{c\to 1},\ \ -\mathbf{i}^T\mathbf{f}^{o3}_{c\to 1} \ \leq\ -\mu\,\mathbf{j}^T\mathbf{f}^{o3}_{c\to 1}, \\ \ \ i = 1,\ldots,q_1, \end{array} \right. \tag{23}$$

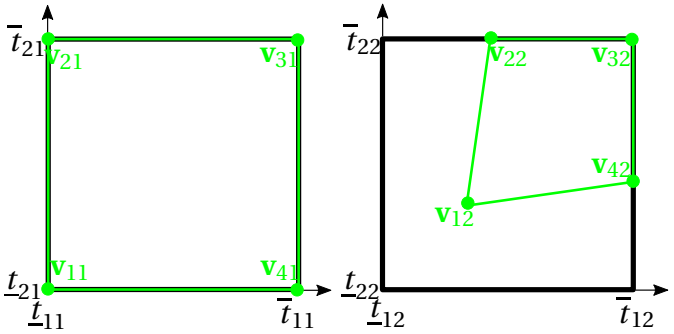

FIGURE 4: CTS formed by cables $\mathscr{C}_{i1}$ (left) and $\mathscr{C}_{i2}$ (right) in the first mode of operation

$$\mathscr{A}_{32} = \left\{ \mathbf{f}_2 \in \mathbb{R}^2 \mid \mathbf{f}_2 = \sum_{i=1}^{q_2} t_{i2}\mathbf{u}^{op3}_{i2},\ \ \underline{t}_{i2} \leq t_{i2} \leq \overline{t}_{i2},\ \ i = 1,\ldots,q_2. \right. \tag{24}$$

Note that $\mathbf{u}^{op3}_{i2}$ differs from to $\mathbf{u}_{i2}$ as shown in Fig. 3d.

4.1 Hyperplane Shifting Method for dual-platform CDPRs

By considering only the classical cable tension limits ($\underline{t}_{ij}$ and $\overline{t}_{ij}$), the shape of the AWS takes the form of a zonotope [25]. However, when considering additional non-sliding conditions, the shape of the AWS becomes a convex polytope, as previously demonstrated in [16]. To define the AWS in our case, the Hyperplane Shifting Method (HFM) is used, which defines a convex polytope as the intersection of the half-spaces bounded by its hyperplanes. This approach is similar to that used in [16], however the constraints are different and must be defined analytically. This AWS is bounded by hyperplanes obtained from the cable tension limits associated to the four cables attached to the point mass moving-platforms, and by the hyperplanes corresponding to the non-sliding conditions derived and explained hereafter.

4.1.1 Hyperplanes associated with the cable tension limits

For classical CDPRs with given cable tension limits, $\Delta t_{ij} = \overline{t}_{ij} - \underline{t}_{ij}$ is a constant, AWS is a zonotope formed by the set of vectors $\alpha_{ij}\Delta t_{ij}\mathbf{u}_{ij}$, where $0 \leq \alpha_{ij} \leq 1$ [25, 26]. The shape of the zonotope depends on the cable unit vectors $\mathbf{u}_{ij}$ as well as the difference between the minimum and maximum cable tension limits Δt_{ij}. It is noteworthy that Δt_{ij} is no longer a constant for dual-platform CDPRs. The property of a zonotope having parallel facets still holds as the orientation of the hyperplanes is given by the cable unit vectors. However, the position of the hyperplanes is modified, forming a convex polytope with parallel facets rather than a zonotope. The hy-

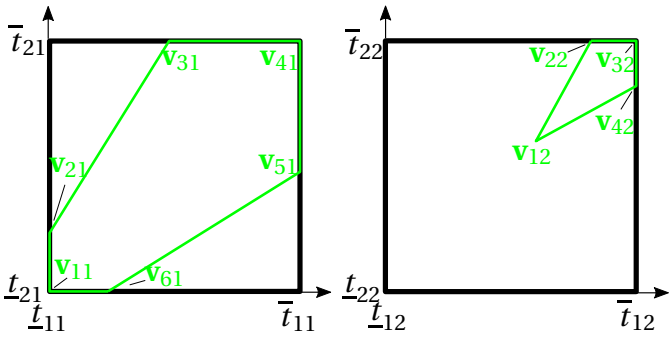

FIGURE 5: CTS formed by cables $\mathscr{C}_{i1}$ (left) and $\mathscr{C}_{i2}$ (right) in the second mode of operation

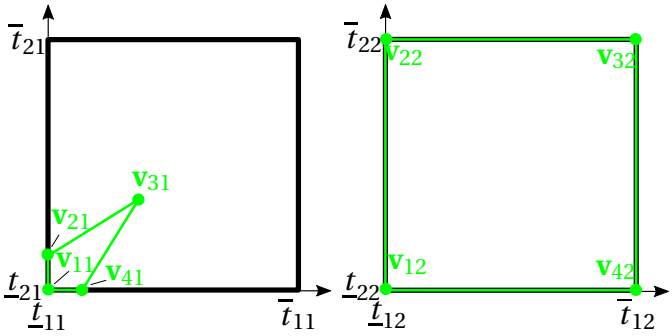

FIGURE 6: CTS formed by cables $\mathscr{C}_{i1}$ (left) and $\mathscr{C}_{i2}$ (right) in the third mode of operation

perplanes associated with the cable tension limits in the presence of additional constraints has been well studied in [27].

The aforementioned hyperplanes can generally be obtained using the Cable Tension Space (CTS) of a CDPR. However, in case of a dual-platform CDPR, for each operation mode, CTS is formed by the vertices, denoted as $\mathbf{v}_{kj},\ k = 1,\ldots,v_j,\ j = 1,2$. v_j denotes the number of vertices for the CTS formed by the cables $\mathscr{C}_{ij},\ i = 1,\ldots,q_j$. The complete CTS for a dual-platform CDPR is obtained by taking the Cartesian product between the vertices $\mathbf{v}_{k1},\ k = 1,\ldots,v_1$ and $\mathbf{v}_{k2},\ k = 1,\ldots,v_2$. Figure 4, 5 and 6 depicts the CTS for the three operation modes for the robot poses shown in Fig 2, respectively.

In the case of a point mass moving-platform, each cable forms a pair of parallel hyperplanes. Each pair is defined by a vector that is orthogonal to its facets, and the shifted distance from the origin that is determined by the projection of the Cable Tension Space (CTS) vertices onto the orthogonal vector. In a case study with $q_1 = q_2 = 2$, there will be a total of eight hyperplanes associated with the cable tension limits. For the additional constraints, each non-sliding condition generates a single hyperplane in the wrench space.

4.1.2 Hyperplanes associated with the First Operation Mode In order to define the hyperplane associated with the non-sliding conditions, the aforementioned constraints must be expressed into the wrench space. For the first operation mode, Eqs. (12) are to be expressed in the wrench space of a dual-platform CDPR. Substituting Eq. (7) into the Eq. (12a) yields:

$$\mathbf{i}^T(-\mathbf{W}_2\mathbf{t}_2 - m_2\mathbf{g}) \ \leq\ -\mu\,\mathbf{j}^T(-\mathbf{W}_2\mathbf{t}_2 - m_2\mathbf{g}). \tag{25}$$

As $\mathbf{i}^T m_2\mathbf{g} = 0$,

$$\left[-\mathbf{i}^T - \mu\,\mathbf{j}^T\right]\mathbf{W}_2\mathbf{t}_2 \ \leq\ \mu\,\mathbf{j}^T m_2\mathbf{g}. \tag{26}$$

In order to map Eq. 26 into the wrench space, we introduce $\mathbf{t}_1$ in addition to $\mathbf{t}_2$. Adding $[-\mathbf{i}^T - \mu\,\mathbf{j}^T]\mathbf{W}_1\mathbf{t}_1$ in the above equation yields:

$$\left[-\mathbf{i}^T - \mu\,\mathbf{j}^T\right](\mathbf{W}_1\mathbf{t}_1 + \mathbf{W}_2\mathbf{t}_2) \ \leq\ \mu\,\mathbf{j}^T m_2\mathbf{g} + \left[-\mathbf{i}^T - \mu\,\mathbf{j}^T\right]\mathbf{W}_1\mathbf{t}_1. \tag{27}$$

Using Eq. (10), the above equation can be expressed in the form :

$$\mathbf{e}_{op1}^{-\,T}\,\mathbf{f} \ \leq\ d_{op1}^{-} \tag{28}$$

where $\mathbf{e}_{op1}^{-}$ is an n-dimensional unit vector defining the facet of the hyperplane and d_{op1}^{-} denotes the shifted distance of the hyperplane from the origin along $\mathbf{e}_{op1}^{-}$, expressed as:

$$\mathbf{e}_{op1}^{-} = \frac{\left[-\mathbf{i}^T - \mu\,\mathbf{j}^T\right]^T}{\|-\mathbf{i}^T - \mu\,\mathbf{j}^T\|}, \tag{29a}$$

$$d_{op1}^{-} = \frac{\mu\,\mathbf{j}^T m_2\mathbf{g} + (-\mathbf{i}^T - \mu\,\mathbf{j}^T)\max\left(\sum_{i=1}^{q_1}\mathbf{u}_{i1}\mathbf{v}_{k1},\ \ k = 1,\ldots,v_1\right)}{\|-\mathbf{i}^T - \mu\,\mathbf{j}^T\|} \tag{29b}$$

Equation (28) expresses the non-sliding condition in Eq. (12a) into the wrench space. Similarly, the non-sliding condition in Eq. (12b) can be expressed in the wrench space as:

$$\mathbf{e}_{op1}^{+\,T}\,\mathbf{f} \ \leq\ d_{op1}^{+} \tag{30}$$

where $\mathbf{e}_{op1}^{+}$ is also an n-dimensional unit vector and d_{op1}^{+} denotes the shifted distance of the hyperplane from the origin of

the wrench space along $\mathbf{e}^+_{op1}$, expressed as:

$$\mathbf{e}^+_{op1} = \frac{\left[\mathbf{i}^T - \mu\,\mathbf{j}^T\right]^T}{\|\mathbf{i}^T - \mu\,\mathbf{j}^T\|}, \tag{31a}$$

$$d^+_{op1} = \frac{\mu\,\mathbf{j}^T m_2\mathbf{g} + (\mathbf{i}^T - \mu\,\mathbf{j}^T)\,\max\left(\sum_{i=1}^{q_1}\mathbf{u}_{i1}\mathbf{v}_{k1},\ \ k=1,\ldots,v_1\right)}{\|\mathbf{i}^T - \mu\,\mathbf{j}^T\|} \tag{31b}$$

Equations (28) and (30) are the two additional hyperplanes that form the AWS of a dual-platform CDPR in the first operation mode.

4.1.3 Hyperplanes associated with the Second Operation Mode As described in Sec. 3.2, the second operation mode is under the influence of two types of non-sliding constraints (Eq.(12) and Eq. (15)). Equation (12) remains the same in the wrench space as expressed by Eqs. (28) and (30). However, in the second mode of operation, we also need to express the constraints in Eq. (15) into the wrench space of a dual-platform CDPR. Substituting Eq. (14) into Eq. (15a) yields:

$$\mathbf{i}^T(-\mathbf{W}\mathbf{t} - (m_1+m_2)\,\mathbf{g}) \;\le\; -\mu\,\mathbf{j}^T(-\mathbf{W}\mathbf{t} - (m_1+m_2)\,\mathbf{g}). \tag{32}$$

As the term $\mathbf{i}^T(m_1+m_2)\mathbf{g} = 0$, substituting Eq.(10) into the Eq.(32) yields:

$$\left[-\mathbf{i}^T - \mu\,\mathbf{j}^T\right]\,\mathbf{f} \;\le\; \mu\,\mathbf{j}^T(m_1+m_2)\mathbf{g} \tag{33}$$

Equation.(33) represents the non-sliding condition in Eq. (15a) into the wrench space. Similarly, Eq.(15b) can also be represented into the wrench space. Both the latter constraints can be written in the form:

$${\mathbf{e}^-_{op2}}^T\mathbf{f} \;\le\; d^-_{op2}, \qquad {\mathbf{e}^+_{op2}}^T\mathbf{f} \;\le\; d^+_{op2}. \tag{34}$$

where $\mathbf{e}^-_{op2}$ ($\mathbf{e}^+_{op2}$, resp.) is an n-dimensional unit vector and d^-_{op2} (d^+_{op2}, resp.) denotes the shifted distance of the hyperplane from the origin of the wrench space along $\mathbf{e}^-_{op2}$ ($\mathbf{e}^+_{op2}$, resp.), expressed as:

$$\mathbf{e}^-_{op2} = \frac{\left[-\mathbf{i}^T - \mu\,\mathbf{j}^T\right]^T}{\|\left[-\mathbf{i}^T - \mu\,\mathbf{j}^T\right]^T\|}, \quad d^-_{op2} = \frac{\mu\,\mathbf{j}^T(m_1+m_2)\,\mathbf{g}}{\|\left[-\mathbf{i}^T - \mu\,\mathbf{j}^T\right]^T\|} \tag{35}$$

$$e^+_{op2} = \frac{\left[\mathbf{i}^T - \mu\,\mathbf{j}^T\right]^T}{\|\left[\mathbf{i}^T - \mu\,\mathbf{j}^T\right]^T\|}, \quad d^+_{op2} = \frac{\mu\,\mathbf{j}^T(m_1+m_2)\,\mathbf{g}}{\|\left[\mathbf{i}^T - \mu\,\mathbf{j}^T\right]^T\|} \tag{36}$$

Equation (34) describes the two additional hyperplanes that, together with the hyperplanes associated with the cable tension limits and the hyperplanes represented by Eq. (28) and (30), form the AWS of a dual-platform CDPR for the second operation mode.

4.1.4 Hyperplanes associated with the Third Operation Mode In the third mode of operation, the only non-sliding condition is associated between the ceiling and $\mathscr{P}_1$ expressed by Eqs. (19) and thus, are required to be expressed into the wrench space $\mathbf{f}_1$ of the platform $\mathscr{P}_1$. Substituting Eq. (18) into the Eq. (19a) yields:

$$\mathbf{i}^T(-\mathbf{W}_1\mathbf{t}_1 - m_1\mathbf{g}) \;\le\; -\mu\,\mathbf{j}^T(-\mathbf{W}_1\mathbf{t}_1 - m_1\mathbf{g}). \tag{37}$$

Note that $\mathbf{i}^T m_j\mathbf{g} = 0$. Substituting Eq.(17) in the Eq.(37) yields:

$$\left[-\mathbf{i}^T - \mu\,\mathbf{j}^T\right]\mathbf{f}_1 \;\le\; \mu\,\mathbf{j}^T m_1\mathbf{g}. \tag{38}$$

Equation (38) represents the non-sliding condition in Eq. (19a) into the wrench space. Similarly, Eq.(19b) can also be represented into the wrench space. Both the latter constraints can be written in the form:

$${\mathbf{e}^-_{op3}}^T\mathbf{f} \le\; d^-_{op3}, \qquad {\mathbf{e}^+_{op3}}^T\mathbf{f} \le\; d^+_{op3}, \tag{39}$$

where $\mathbf{e}^-_{op3}$ ($\mathbf{e}^+_{op3}$, resp.) is an n-dimensional unit vector and d^-_{op3} (d^+_{op3}, resp.) denotes the shifted distance of the hyperplane from the origin of the wrench space along $\mathbf{e}^-_{op3}$ ($\mathbf{e}^+_{op3}$, resp.), expressed as:

$$\mathbf{e}^-_{op3} = \frac{\left[-\mathbf{i}^T - \mu\,\mathbf{j}^T\right]^T}{\|\left[-\mathbf{i}^T - \mu\,\mathbf{j}^T\right]^T\|}, \quad d^-_{op3} = \frac{\mu\,\mathbf{j}^T m_1\mathbf{g}}{\|\left[-\mathbf{i}^T - \mu\,\mathbf{j}^T\right]^T\|} \tag{40}$$

$$\mathbf{e}^+_{op3} = \frac{\left[\mathbf{i}^T - \mu\,\mathbf{j}^T\right]^T}{\|\left[\mathbf{i}^T - \mu\,\mathbf{j}^T\right]^T\|}, \quad d^+_{op3} = \frac{\mu\,\mathbf{j}^T m_1\mathbf{g}}{\|\left[\mathbf{i}^T - \mu\,\mathbf{j}^T\right]^T\|} \tag{41}$$

Equation (39) outlines the two additional hyperplanes that, in combination with the hyperplanes related to cable tension constraints, form the AWS for the third operation mode of a

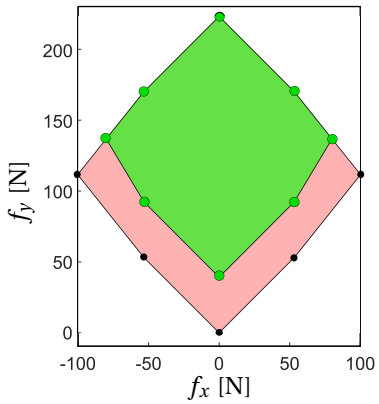

(a) Change in the AWS of the CDPR in the first mode of operation

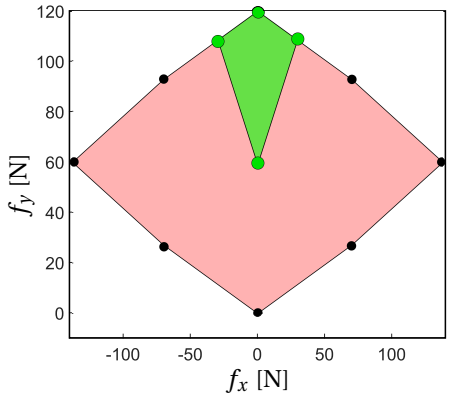

(b) Change in the AWS of the CDPR in the second mode of operation

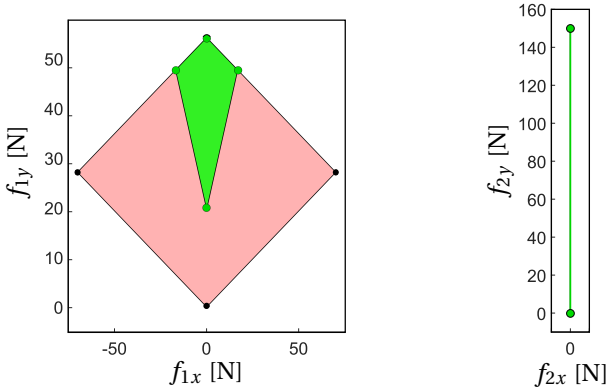

(c) Change in the AWS of the CDPR in the third mode of operation for the platform $\mathscr{P}_1$ (left) and the platform $\mathscr{P}_2$ (right)

FIGURE 7: AWS of a dual-platform CDPR for each mode of operation in Fig. 2 for $\mu = 0.5$

dual-platform CDPR. Figure 7 illustrates the AWS for each operation mode depicted in Fig.2 with m_1 = 2kg and m_2 = 4kg. The AWS of the classical CDPR, without any supplementary constraints, is displayed in red, while the AWS incorporating the additional non-sliding constraints is depicted in green. It can be seen that the additional non-sliding conditions significantly limit the robot's wrench capabilities. In Fig.7a, the minimum possible wrench that can be generated by the cables onto the moving-platform is equal to the weight of $\mathscr{P}_2$, as compelled by the right-hand side of the constraint in Eq.11. Similar phenomena can be observed in the second(Fig.7b) and third(Fig. 7c) operation modes. These results indicate that the platforms may lose contact if the wrenches generated by the cables fall below certain thresholds defined by the weights of the moving-platforms.

5 Workspace Analysis

An important design consideration that requires investigation is the wrench feasible workspace (WFW), which is particularly relevant to the first mode of operation. It is imperative to identify a workspace that is capable of keeping both platforms in contact while ensuring that the required wrenches can be sustained. Therefore, the WFW of the planar dual-platform CDPR is investigated in this section. It is defined as the set of moving-platform poses that are wrench-feasible [28, 29]. A well known index used to compute the wrench feasible set of poses is called Capacity Margin [30]. It is a measure of the robustness of the equilibrium of the robot. The static WFW of the platform under study is presented in Fig. 8 for the first operation mode. The green region corresponds to the area where both cable tension limits and non-sliding constraints are satisfied. On the other hand, the red area corresponds to the WFW of a classical CDPR that only takes into account cable tension limits. It can be seen that for the dual-platform CDPRs, the ability of the cables to apply wrenches may be reduced due to the additional non-sliding constraints. It has been observed that a convergence between the green and red regions is highly unlikely, even if the friction coefficient μ tends to infinity, as the weight of the platforms will always impose limitations on the platform wrench capability.

6 Conclusion and Future Work

In this paper, a methodology to obtain the Wrench-Feasible-Workspace for a composite Cable-Driven Parallel Robots was introduced. Three operation modes of dual-platform Cable-Driven Parallel Robots were defined. For each operation mode, it was shown that the Available Wrench Set depends on both the static equilibrium of the moving-platforms and contact conditions. The proposed method was validated in simulation. Future work will focus on an extension of this work to spatial mechanisms with surface contact

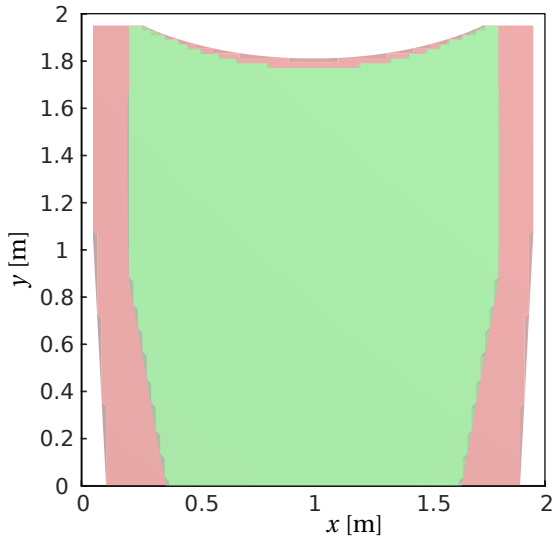

(a) WFW with $\mu = 0.1$

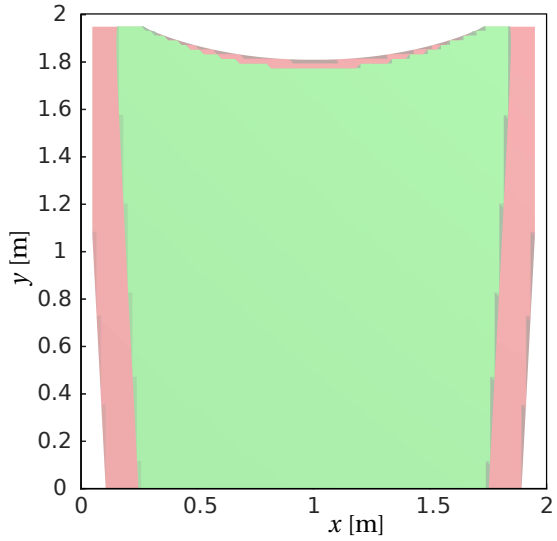

(b) WFW with $\mu = 10$

FIGURE 8: Wrench Feasible Workspace of the planar dual-platform CDPR in the first mode of operation

conditions and experimental validations by using the prototype shown in Fig.1.

ACKNOWLEDGMENT

This work was supported by the ANR CRAFT project, France, grant ANR-18-CE10-0004, https://anr.fr/Project-ANR-18-CE10-0004. This work has been partially supported by ROBOTEX 2.0 (Grants ROBOTEX ANR-10-EQPX-44-01 and TIRREX ANR-21-ESRE-0015).

REFERENCES

[1] Kawamura, S., and Ito, K., 1993. "A new type of master robot for teleoperation using a radial wire drive system". In Proceedings of 1993 IEEE/RSJ International Conference on Intelligent Robots and Systems (IROS'93), Vol. 1, IEEE, pp. 55–60.

[2] Lambert, C., Nahon, M., and Chalmers, D., 2007. "Implementation of an aerostat positioning system with cable control". *IEEE/ASME Transactions on Mechatronics,* ***12***(1), pp. 32–40.

[3] Pedemonte, N., Rasheed, T., Marquez-Gamez, D., Long, P., Hocquard, É., Babin, F., Fouché, C., Caverot, G., Girin, A., and Caro, S., 2020. "Fastkit: A mobile cable-driven parallel robot for logistics". In *Advances in Robotics Research: From Lab to Market*. Springer, pp. 141–163.

[4] Chen, Q., Zi, B., Sun, Z., Li, Y., and Xu, Q., 2019. "Design and development of a new cable-driven parallel robot for waist rehabilitation". *IEEE/ASME Transactions on Mechatronics,* ***24***(4), pp. 1497–1507.

[5] Aref, M. M., and Taghirad, H. D., 2008. "Geometrical workspace analysis of a cable-driven redundant parallel manipulator: Kntu cdrpm". In 2008 IEEE/RSJ International Conference on Intelligent Robots and Systems, IEEE, pp. 1958–1963.

[6] Wischnitzer, Y., Shvalb, N., and Shoham, M., 2008. "Wire-driven parallel robot: Permitting collisions between wires". *The International Journal of Robotics Research,* ***27***(9), pp. 1007–1026.

[7] Blanchet, L., and Merlet, J.-P., 2014. "Interference detection for cable-driven parallel robots (cdprs)". In 2014 IEEE/ASME International Conference on Advanced Intelligent Mechatronics, IEEE, pp. 1413–1418.

[8] Nguyen, D. Q., and Gouttefarde, M., 2015. "On the improvement of cable collision detection algorithms". In *Cable-Driven Parallel Robots*. Springer, pp. 29–40.

[9] Lahouar, S., Ottaviano, E., Zeghoul, S., Romdhane, L., and Ceccarelli, M., 2009. "Collision free path-planning for cable-driven parallel robots". *Robotics and Autonomous Systems,* ***57***(11), pp. 1083–1093.

[10] Bak, J.-H., Hwang, S. W., Yoon, J., Park, J. H., and Park, J.-O., 2019. "Collision-free path planning of cable-driven parallel robots in cluttered environments". *Intelligent Service Robotics,* ***12***(3), pp. 243–253.

[11] Zhang, B., Shang, W., and Cong, S., 2018. "Optimal rrt* planning and synchronous control of cable-driven parallel robots". In 2018 3rd international conference on advanced robotics and mechatronics (ICARM), IEEE, pp. 95–100.

[12] Tadokoro, S., Matsushima, T., Murao, Y., and Kohkawa, H., 2001. "A parallel cable-driven motion base for virtual acceleration". In Proceedings 2001 IEEE/RSJ International Conference on Intelligent Robots and Systems. Expand-

ing the Societal Role of Robotics in the the Next Millennium (Cat. No. 01CH37180), Vol. 3, IEEE, pp. 1700–1705.

[13] Izard, J.-B., Gouttefarde, M., Michelin, M., Tempier, O., and Baradat, C., 2013. "A reconfigurable robot for cable-driven parallel robotic research and industrial scenario proofing". In *Cable-driven parallel robots*. Springer, pp. 135–148.

[14] Gagliardini, L., Caro, S., Gouttefarde, M., and Girin, A., 2016. "Discrete reconfiguration planning for cable-driven parallel robots". *Mechanism and Machine Theory,* ***100***, pp. 313–337.

[15] Tan, H., Nurahmi, L., Pramujati, B., and Caro, S., 2020. "On the reconfiguration of cable-driven parallel robots with multiple mobile cranes". In 2020 5th International Conference on Robotics and Automation Engineering (ICRAE), IEEE, pp. 126–130.

[16] Rasheed, T., Long, P., Marquez-Gamez, D., and Caro, S., 2018. "Available wrench set for planar mobile cable-driven parallel robots". In 2018 IEEE International Conference on Robotics and Automation (ICRA), IEEE, pp. 962–967.

[17] Rasheed, T., Long, P., Marquez-Gamez, D., and Caro, S., 2018. "Tension distribution algorithm for planar mobile cable-driven parallel robots". In *Cable-Driven Parallel Robots*. Springer, pp. 268–279.

[18] Rasheed, T., Long, P., Roos, A. S., and Caro, S., 2019. "Optimization based trajectory planning of mobile cable-driven parallel robots". In 2019 IEEE/RSJ International Conference on Intelligent Robots and Systems (IROS), IEEE, pp. 6788–6793.

[19] Xu, J., Kim, B.-G., and Park, K.-S., 2022. "A collaborative path planning method for mobile cable-driven parallel robots in a constrained environment with considering kinematic stability". *Complex & Intelligent Systems*, pp. 1–12.

[20] Skopin, M., Long, P., and Padir, T., 2021. "Design of a docking system for cable-driven parallel robot to allow workspace reconfiguration in cluttered environments". In International Conference on Cable-Driven Parallel Robots, Springer, pp. 158–169.

[21] Schultz, H., 1974. Retractable pen, June 25. US Patent 3,819,282.

[22] Hiller, M., Fang, S., Mielczarek, S., Verhoeven, R., and Franitza, D., 2005. "Design, analysis and realization of tendon-based parallel manipulators". *Mechanism and Machine Theory,* ***40***(4), pp. 429–445.

[23] Samy, V., Caron, S., Bouyarmane, K., and Kheddar, A., 2017. "Adaptive compliance in post-impact humanoid falls using preview control of a reduce model".

[24] Caron, S., Pham, Q.-C., and Nakamura, Y., 2016. "Zmp support areas for multicontact mobility under frictional constraints". *IEEE Transactions on Robotics,* ***33***(1), pp. 67–80.

[25] Bouchard, S., Gosselin, C., and Moore, B., 2010. "On the ability of a cable-driven robot to generate a prescribed set of wrenches".

[26] Gouttefarde, M., and Krut, S., 2010. "Characterization of parallel manipulator available wrench set facets". In Advances in Robot Kinematics: Motion in Man and Machine: Motion in Man and Machine, Springer, pp. 475–482.

[27] Rasheed, T., Long, P., and Caro, S., 2020. "Wrench-feasible workspace of mobile cable-driven parallel robots". *Journal of Mechanisms and Robotics,* ***12***(3).

[28] Bosscher, P., Riechel, A. T., and Ebert-Uphoff, I., 2006. "Wrench-feasible workspace generation for cable-driven robots". *IEEE Transactions on Robotics,* ***22***(5), pp. 890–902.

[29] Cruz Ruiz, A. L., Caro, S., Cardou, P., and Guay, F., 2015. "ARACHNIS: Analysis of Robots Actuated by Cables with Handy and Neat Interface Software". In *Cable-Driven Parallel Robots, Mechanisms and Machine Science*, Vol. 32 of *Mechanisms and Machine Science*. Springer, Jan., pp. 293–305.

[30] Guay, F., Cardou, P., Cruz-Ruiz, A. L., and Caro, S., 2014. "Measuring how well a structure supports varying external wrenches". In New Advances in Mechanisms, Transmissions and Applications: Proceedings of the Second Conference MeTrApp 2013, Springer, pp. 385–392.